

NUMERICAL STUDY OF HYDRODYNAMICS AND MASS TRANSFER OF IN-LINE FIBER ARRAYS IN LAMINAR CROSS-FLOW

T. LI, N.G. DEEN and J.A.M. KUIPERS

Faculty of Science and Technology, University of Twente,
P.O. Box 217, 7500 AE Enschede, THE NETHERLANDS

ABSTRACT

In this paper the hydrodynamics and shell side mass transfer of laminar flow across in-line tube arrays is studied numerically. The hydrodynamics of a five-tube array were described by the two-dimensional Navier-Stokes equations, employing the stream function-vorticity method. After a converged solution for the hydrodynamics had been found, a transport equation for the concentration was solved. The numerical grid of the investigated geometries consists of a number of basic cells, which are generated with a domain decomposition method combined with orthogonal grid generation. The hydrodynamics and mass transfer were analysed for Reynolds = 2-200, Péclet = 10-300 and pitch-to-diameter ratios of 1.5, 1.85 and 2.0. It is shown that the strength of the recirculation occurring between the adjacent tubes increases with increasing Reynolds number, and with decreasing pitch-to-diameter ratio.

NOMENCLATURE

x, y	Cartesian coordinates
A	tube radius
C	concentration
c	dimensionless concentration
D	diffusivity
f	distortion function
h_η, h_ξ	scalar factor
Pe	Péclet number
Re	Reynolds number
Sc	Schmidt number
Sh	Sherwood number
U_∞	bulk velocity

Greek symbols

ψ	stream function
ω	vorticity
ξ, η	computational coordinates
λ	pitch-to-diameter ratio
ν	kinematic viscosity

Subscripts

$avg.$	Average
b	bulk
in	inlet
loc	local
t	tube

INTRODUCTION

Due to their excellent mass transfer properties hollow fiber membrane modules are extensively used in many applications such as absorption, extraction, osmosis and ultrafiltration. One of the most commonly used hollow fiber geometries is the shell and tube configuration with a bundle of hundreds of porous fibers, aligned axially but arranged orderly or randomly in the cross section (Wu and Chen, 2000). Many experimental studies have been published on mass transfer in hollow fiber modules. The mass transfer inside hollow fibers can be described analytically due to the relatively simple flow conditions: laminar flow with a parabolic velocity profile. On the other hand, empirical correlations are mostly used for the prediction of the mass transfer coefficient at the shell-side of hollow fiber membranes (Yang and Cussler, 1986, Wickramasinghe *et al.*, 1993, Costello, *et al.*, 1993). The experimental studies have led to practical correlations but not to detailed insight and understanding of the underlying phenomena. In this respect an approach based on computational fluid dynamics can serve as an important complementary tool to experimental approaches.

Although relatively little numerical work has been done on mass transfer in these particular systems, there is a vast amount of numerical work in the area of heat transfer in shell and tube heat exchangers, which is analogous to mass transfer in tube bundles due to the Chilton-Colburn analogy. Numerical work on mass transfer in tube bundles and related work for heat transfer will now briefly be reviewed.

Baier *et al.* (1999) investigated the mass transfer rates in spatially periodic flows through staggered arrays. In their method the velocity field was obtained numerically using the creeping flow assumption whereas the mass transfer coefficients were obtained using boundary layer theory. The drawback of their method is that the influence of the boundary layer thickness caused by the recirculation between the adjacent tubes inside the array, cannot be correctly taken into account. The calculation procedure is therefore limited to the range of creeping flow. Bao & Lipscomb (2002) analyzed the mass transfer in axial flows through randomly packed fiber bundles with uniform wall flux. The finite element method was used to solve governing momentum and conservation of mass equations in their prediction. One of the limitations of their method is that it cannot be applied to the cross flow fiber module that is more complex than the axial flow module.

Several studies on the numerical simulation of hydrodynamics and heat transfer of flow through tube banks have been published year to year (Lauder & Massey, 1978, Chen & Wung, 1989 and Wung & Chen,

1989). It was reported that heat transfer coefficients in the shell-side of cross flow units are higher than those in parallel units in all the test cases. Furthermore, Schöner *et al.* (1998) found that the transfer processes are additionally faster when the hollow fibers are evenly spaced in modules.

The objective of the present investigation is limited to the simulation of mass transfer in in-line hollow fiber tube arrays subjected to cross flow. This paper consists of three parts. The first part describes the mathematical model and its numerical procedure. In the second part numerical results are presented and analysed in detail. Finally the conclusions are presented.

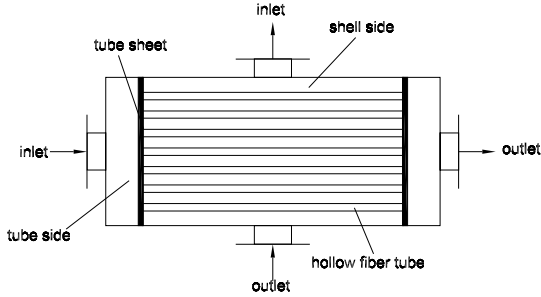


Figure 1: Typical structure of the cross-flow hollow-fiber contactor

MODEL DESCRIPTION

The structure of a typical cross-flow hollow fiber contactor is illustrated in Fig. 1. During the operation one fluid containing a dissolved component flows through the tube side (or shell side), while the other fluid flows across the shell-side (or tube-side) separately. Usually a distributor is installed near the inlet side to facilitate proper contacting with the tube array. Efficient exchange of the dissolved component between the two fluids (i.e. liquid/liquid or gas/liquid) can be achieved through the high specific area.

For modeling of mass transfer in these cross flow modules not only the knowledge of the mass transfer inside the tubes but also the knowledge of the mass transfer at the shell side is necessary (Shröner *et al.*, 1998). In this study we will focus on the mass transfer phenomena at the shell side using a two-dimensional model. The Navier-Stokes and species conservation equations are given below in curvilinear coordinates (Li, 1998):

$$\frac{\partial \omega}{\partial t} + \frac{1}{h_\xi h_\eta} \left[\frac{\partial}{\partial \xi} \left(\frac{\partial \psi}{\partial \eta} \omega \right) - \frac{\partial}{\partial \eta} \left(\frac{\partial \psi}{\partial \xi} \omega \right) \right] = \quad (1)$$

$$\frac{2}{\text{Re}} \frac{1}{h_\xi h_\eta} \left[\frac{\partial}{\partial \xi} \left(f \frac{\partial \omega}{\partial \xi} \right) + \frac{\partial}{\partial \eta} \left(\frac{1}{f} \frac{\partial \omega}{\partial \eta} \right) \right]$$

$$\frac{1}{h_\xi h_\eta} \left[\frac{\partial}{\partial \xi} \left(f \frac{\partial \psi}{\partial \xi} \right) + \frac{\partial}{\partial \eta} \left(\frac{1}{f} \frac{\partial \psi}{\partial \eta} \right) \right] = -\omega \quad (2)$$

$$\frac{\partial c}{\partial t} + \frac{1}{h_\xi h_\eta} \left[\frac{\partial}{\partial \xi} \left(\frac{\partial \psi}{\partial \eta} c \right) - \frac{\partial}{\partial \eta} \left(\frac{\partial \psi}{\partial \xi} c \right) \right] = \quad (3)$$

$$\frac{2}{\text{Pe}} \frac{1}{h_\xi h_\eta} \left[\frac{\partial}{\partial \xi} \left(f \frac{\partial c}{\partial \xi} \right) + \frac{\partial}{\partial \eta} \left(\frac{1}{f} \frac{\partial c}{\partial \eta} \right) \right]$$

where $x = x(\xi, \eta)$, $y = y(\xi, \eta)$.

The influence of dissolved components on the flow behavior is negligible at low concentration and as a consequence Eq. (3) can be decoupled from Eqs. (1) and (2) when carrying out the mass transfer calculations. However Eqs. (1) and (2) must be simultaneously solved by iteration. Note that in the governing equations the time terms are retained in Eqs. (1) and (3) as a pseudo time for convenience of the solver.

The dimensionless quantities are listed below; for notation convenience the superscripts are omitted in the transport equations.

$$\omega' = a\omega/U_\infty, \quad \psi' = \psi/aU_\infty, \quad t' = tU_\infty/a, \quad (4)$$

$$\xi' = \xi/a, \quad \eta' = \eta/a, \quad c' = (c - c_{in})/(c_s - c_{in})$$

The dimensionless Reynolds, Péclet and Schmidt numbers are defined as:

$$\text{Re} = 2aU_\infty/\nu \quad (5)$$

$$\text{Pe} = \text{Re} \cdot \text{Sc}$$

$$\text{Sc} = \nu/D \quad (6)$$

For solution of the species conservation equation some assumptions must be made: the tube surface always has a uniform constant concentration and its variation along the axis direction of the tube array is negligible. The boundary conditions in the physical domain are depicted in Fig. 2 and given below in more detail.

On the inlet AC:

$$\psi(y) = \int_A^B u(y) dy = U_\infty \int_A^B dy, \quad \omega = c = 0 \quad (7)$$

On the outlet BD:

$$\partial \psi / \partial x = \partial \omega / \partial x = \partial c / \partial x = 0 \quad (8)$$

On the symmetry lines AB and CD:

$$\psi = \omega = 0, \quad \partial c / \partial y = 0 \quad (9)$$

On the surface of the cylinders:

$$\psi = 0, \quad \omega = \omega_{\text{surface}}, \quad c = 1 \quad (10)$$

where x and y respectively represent the normal and tangent coordinates.

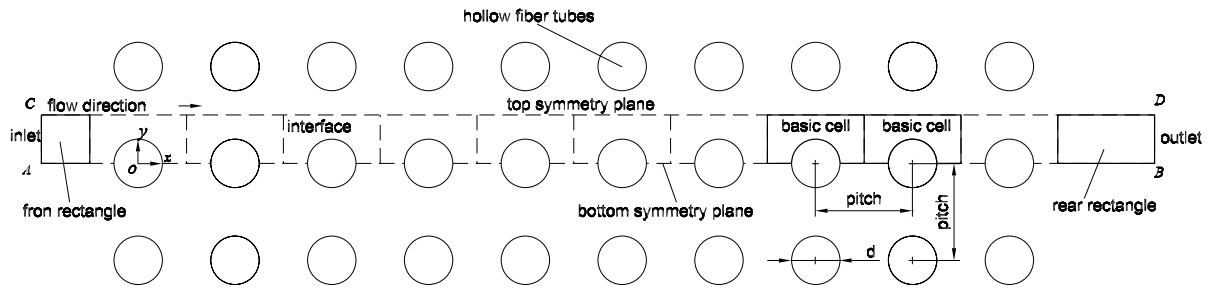


Figure 2: Boundary conditions of stream function, vorticity and concentration in the contactor of in-line array

A domain decomposition method combined with orthogonal grid generation was applied to setup a basic cell that was used serially to carry out the computations on arrays of a tube array. It was shown by Li *et al.* (2004a) that the periodic property of the flow field can be used to extend the computational domain size in the mass transfer simulation, that is to say, large arrays of tubes can be calculated by the present technique.

Further details on the numerical solver algorithm can be found in the work of Li *et al.* (2004a, b).

RESULTS

In general the concentration distribution in the tube array is a strong function of Reynolds number and Schmidt number. The variation of flow and concentration fields at different Schmidt numbers are illustrated by the contours of streamlines and concentration in Figure 4 for $\lambda = 1.5$ and $Re = 40$. As expected, the concentration distribution is mainly dominated by diffusion at low Schmidt numbers, while at high Schmidt numbers convective mass transport plays a major role. From Figure 4 it can also be seen that in the first layer of tubes, where the contour lines are densest near the front of the tube, intensive lateral transport takes place. The contours in the recirculation zones between adjacent pairs of tubes get less dense.

Finally the concentration profiles behind the last tube are different from those in the other layers, implying that the wake behind the rear layer has a stronger effect on the mass transport than that of recirculation between adjacent tubes. In other words, the tubes adjacent to the inlet and outlet cannot be neglected and periodic boundary conditions cannot be applied in solving the mass transport equation. The development of concentration contours follows that of the streamlines, because the evolution of the concentration boundary layer growth commences at the first layer of tubes. For the other layers, low velocity recirculating flow interacts with parts of the front half of subsequent tubes. It can also be seen from the plots that the concentration contours get dense only in those regions where the flow has not separated.

In order to observe the impact of pitch-to-diameter ratio on the concentration fields, the concentration contours at $\lambda = 1.5, 1.85$ and 2.0 at $Re = 100$ and $Sc = 1.0$ are presented together with their corresponding streamlines. There are no clear differences except that the contours become less dense in between the tubes, because with increasing λ the recirculation space becomes larger, which decreases the strength of the recirculation, and consequently reduces the convective mass transport.

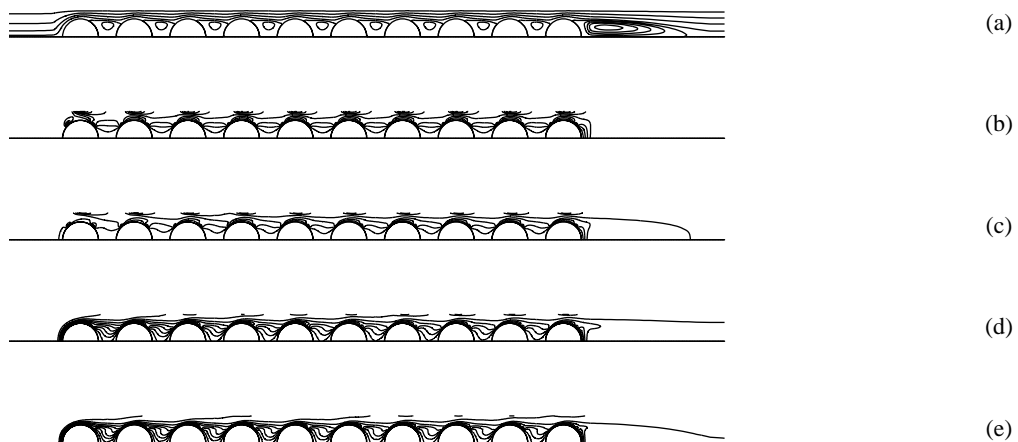


Figure 3: Streamlines (a) and concentration contours at different Sc , (b) 0.25, (c) 1.0, (d) 2.5 and (e) 5.0 with $Re = 40$, $\lambda = 1.5$

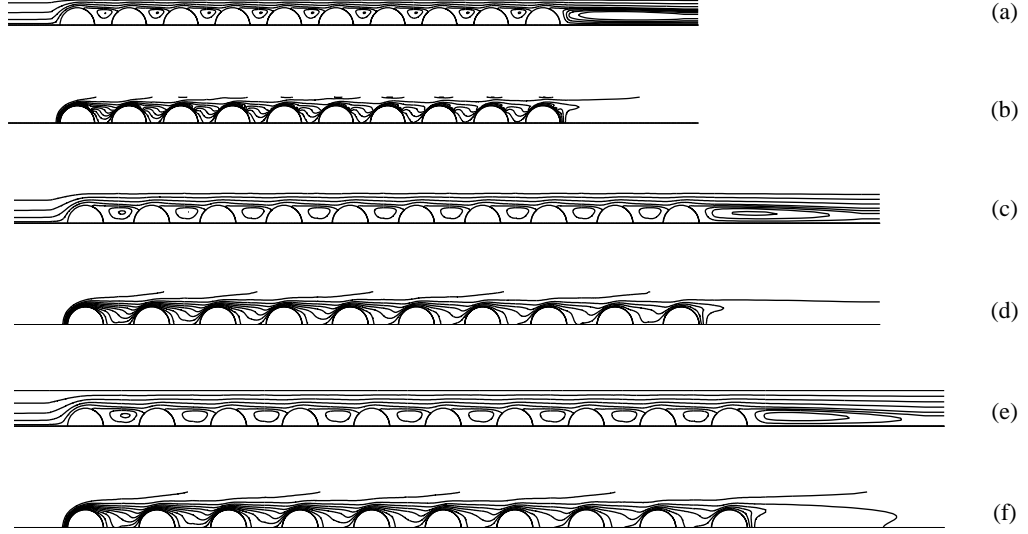


Figure 4: Streamlines (a), (c) and (e) and concentration contours (b), (d) and (f) corresponding to $\lambda = 1.5, 1.85$ and 2.0 at $Re = 100$ and $Sc = 1.0$



Figure 5: Concentration contours at $Re = 200, Sc = 0.5$ with $\lambda = 2.0$

For the same Péclet number, the influence of the flow field on the concentration distribution can be assessed by comparing the concentration contours of Figure 4 (f) with Figure 5. In each of these cases $Pe = 100$, and the concentration distributions in these figures are very similar, except in the vortex region where the latter case shows a stronger recirculation. This phenomenon is very similar to the heat transfer process described by Wung and Chen (1989).

Mass Transfer Analysis

The species concentration contours can provide some detailed information about the development of the concentration fields inside hollow fiber membrane modules. For the design of these units the mass transfer rate from or to the tube surfaces is of key importance. The mass transfer rate can conveniently be expressed in dimensionless form via the Sherwood number. The local Sherwood number is defined as:

$$Sh_{loc} = \frac{2ak_{loc}}{D} = 2 \frac{\sigma}{h_\eta} \frac{\partial c}{\partial \eta} \Big|_{\eta=0} \quad (11)$$

where σ is the dimensionless concentration:

$$\sigma = \frac{c_t - c_{in}}{c_t - c_b} \quad (12)$$

where k_{loc} is mass transfer coefficient, h_η is a scale factor on the tube surface in normal direction. The bulk

concentration, c_b , sometimes called the mixing cup concentration, is defined as:

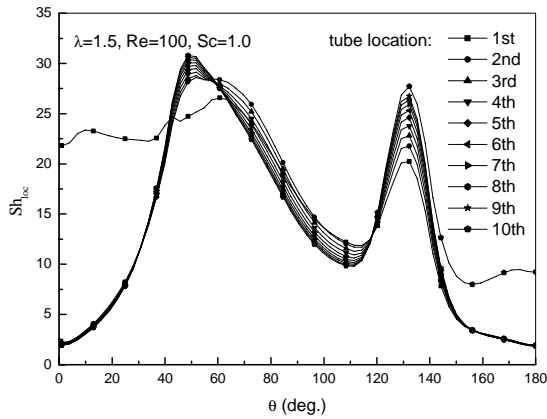
$$c_b = \frac{\int_0^1 c \psi_\eta d\eta}{\int_0^1 \psi_\eta d\eta} \quad (13)$$

in which $d\eta$ is the infinitesimal length along the cross section of the mass transfer direction. The position of bulk concentration in the present study is defined at the minimum cross section similar to the bulk temperature defined by Krishne Gowda *et al.* (1998).

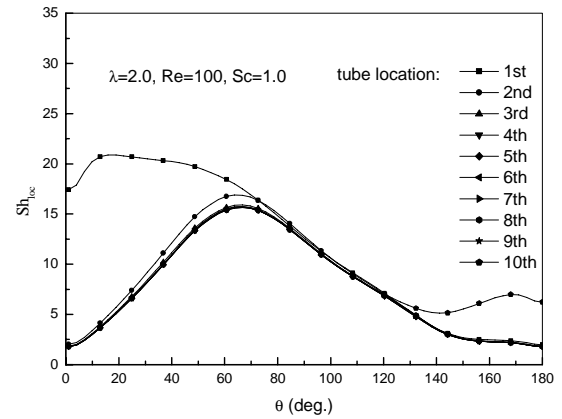
Many factors affect the mass transfer rate between the fluid and the fibers. In the following discussion we will focus only at the most important factors.

Local Mass Transfer Coefficients

The local Sherwood number variations along the tube surface are shown in Figure 6. We will discuss them consecutively. From Figure 6 (a) it can be seen that the profile of Sh_{loc} differs significantly from the corresponding profiles for the other tubes. This is expected because the first tube contacts the incoming fresh fluid and therefore the local Sherwood number is higher than the other tubes in the array. In the vicinity of the front stagnation point of the first tube the concentration gradient is so high that the local mass transfer coefficient reaches its maximum at a small angle and then gradually decreases to the separation point. The spatial variations of local Sherwood numbers for the other tubes are quite similar except for the rear stagnation point of the last tube.



(a)



(b)

Figure 6: The variation of local Sherwood number along each tube surface at different λ .

The peak of the local Sherwood number is pushed backwards to an angle of about 60° from the front stagnation point. Due to recirculation the transferred component recycles between the adjacent tubes and cannot be transported downstream as quickly as in the bulk flow. The spatial distribution of the local Sherwood number along the last tube exhibits a small difference near the separation point since in the rear wake the transferred component can be brought downstream easier, which enhances the mass transfer somewhat.

In order to obtain a thorough understanding of the variation of local mass transfer coefficient of each tube in Figure 6 the curves of Sh_{loc} distribution of the 10-tube array are plotted with $\lambda = 1.5$ and 2.0 . It can be seen that the difference of the local Sherwood number along the consecutive tubes gradually reduces, especially at $\lambda = 1.5$ the variations of local Sherwood number have the same trend.

The main difference between the profiles of local Sherwood number at $\lambda = 1.5$ and 2.0 , is that near the separation point an evident peak appears for $\lambda = 1.5$. This can be explained by the fact that at shorter distances between the tubes, the recirculation is enhanced. This in turn reinforces the mass transfer. This phenomenon can be better understood by considering the concentration boundary layers shown in Figure 7 and Figure 8. On the front of the first tube a very thin concentration boundary layer is set up since the oncoming fresh fluid is free of mass component. The maximum of the local Sherwood number appears within this area. For low values of λ , the fluid close to the separation point is transported away from the cylinder at a relatively high velocity. This leads to high concentration gradients and subsequently to large values of the local Sherwood number. After the separation point the concentration boundary layer thickness is gradually increasing under the influence of the recirculation.

Comparing the thickness of the concentration boundary layers shown in Figure 7 and Figure 8, it can be observed that the concentration boundary layers are thinner at lower

values of the pitch-to-diameter ratio. These features explain why at the same flow condition the mass transfer coefficient decreases with decreasing λ (see also Figure 6). Note that the curves of the first tube shown in Figure 6 are also quite similar to the simulation results of Baier *et al.* (1999), who applied a boundary layer technique to staggered tube arrays.

CONCLUSION

In this paper, numerical predictions of mass transfer at the shell side in in-line hollow fiber tube arrays subject to cross-flow are presented. The computational grid was obtained through a domain decomposition method combined with orthogonal grid generation.

Though the mass transfer is affected by many factors, such as the hydrodynamics, the number of tubes and the tube length etc, we focused our attention only on the influence of hydrodynamics and the pitch-to-diameter ratio on the mass transfer in the present study.

The analysis of the variation of concentration field demonstrates that when diffusion is dominant in the mass transfer the concentration field tends to be relatively homogeneous, whereas when convection is dominant the concentration field differs considerably along the downstream direction.

It was shown that the mass transfer coefficient decreases drastically after the front tube with the increase of tube number along the longitudinal direction especially after the first tubes, but tends to a stable decrease. The numerical predictions show that the mass transfer coefficient is a strong function of Reynolds number, Schmidt number and pitch-to-diameter ratio. The mass transfer coefficient is increased with increase of Reynolds number and Schmidt number, but with decrease of pitch-to-diameter ratio.

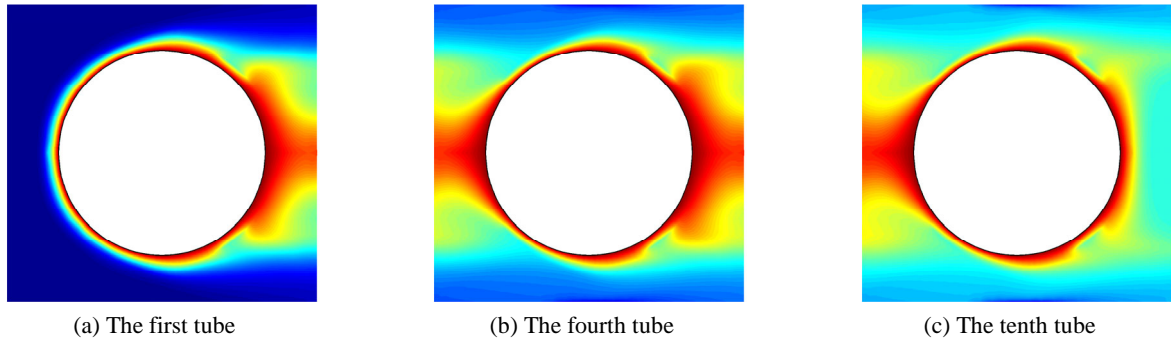


Figure 7: The concentration boundary layer on the tube surface at $\lambda = 1.5$, the blue colour represents the fresh flow and the red colour the concentration on the tube surface.

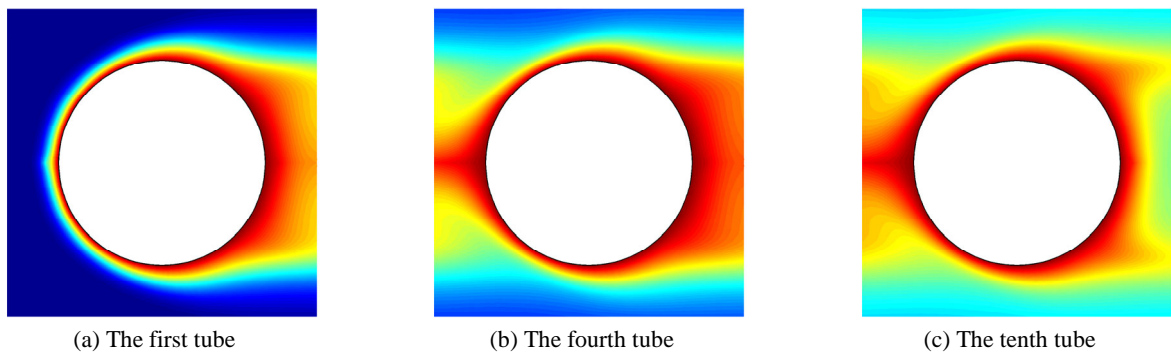


Figure 8: The concentration boundary layer on the tube surface at $\lambda = 2.0$, the blue colour represents the fresh flow and the red colour the concentration on the tube surface.

REFERENCES

- BAIER, G., GRATEFUL, T.M., GRAHAM, M.D. & LIGHTFOOT, E.N. (1999), "Prediction of mass transfer rates in spatially periodic flows", *Chem. Eng. Sci.*, **54**, 343-355.
- BAO, L. & LIPSCOMB, G.G. (2002), "Well-developed mass transfer in axial flows through randomly packed fiber bundles with constant wall flux", *Chem. Eng. Sci.*, **57**, 125-32.
- CHEN, C.J. & WUNG, T.S. (1989), "Finite analytic solution of convective heat transfer for tube arrays in crossflow: Part II-Heat transfer analysis", *ASME J. Heat Transfer*, **111**, 641-648.
- COSTELLO, M.J., FANE, A.G., HOGAN, P.A. and SCHOFIELD, R.W. (1993), "The effect of shell side hydrodynamics on the performance of axial flow hollow fiber modules", *J. Membr. Sci.* **80**, 1-11.
- KRISHNE GOWDA, Y.T., PATNAIK, B.S.V.P., ASWATHA NARAYANA, P.A. & SEETHARAMU, K.N. (1998), "Finite element simulation of transient laminar flow and heat transfer past an in-line tube bank", *Int. J. Heat Fluid Flow*, **19**, 49-55.
- LAUNDER, B.E. & MASSEY, T.H. (1978), "The numerical predictions of viscous flow and heat transfer in tube bank.", *J. Heat Transfer*, **100**, 565-571.
- LI, T., DEEN, N.G. & KUIPERS, J.A.M. (2004a), "Numerical Investigation of Hydrodynamics and Mass Transfer for In-Line Fiber Arrays in Laminar Cross-flow at Low Reynolds Numbers Part I: Hydrodynamics Analysis", *Chem. Eng. Sci.*, in preparation.
- LI, T., DEEN, N.G. & KUIPERS, J.A.M. (2004b), "Numerical Investigation of Hydrodynamics and Mass Transfer for In-Line Fiber Arrays in Laminar Cross-flow at Low Reynolds Numbers Part II: Mass Transfer Simulation", *Chem. Eng. Sci.*, in preparation.
- LI, T. (1998), "Numerical Investigation of hydrodynamics and mass transfer on deformable single drops flowing through a quiescent liquid phase", Doctoral thesis, Institute of Chemical Metallurgy, Chinese Academy of Sciences.
- SCHÖNER, P., PLUCINSKI, W.N. & DAIMINGER, U. (1998), "Mass transfer in the shell side of cross flow hollow fiber modules", *Chem. Eng. Sci.* **53**, 2319-2326..
- WICKRAMASINGHE, S.R., SEMEENS, M.J. and CUSSLER, E.R. (1993), "Hollow fiber modules made with hollow fiber fabric", *J. Membr. Sci.* **84**, 1-5.
- WU, J. and CHEN, V. (2000), "Shell-side mass transfer performance of randomly packed hollow fiber modules", *J. Membr. Sci.* **172**, 59-74.
- WUNG, T.S. & CHEN, C.J. (1989), "Finite analytic solution of convective heat transfer for tube arrays in crossflow: Part I—Flow field analysis", *ASME J. Heat Transfer*, **111**, 633-640.
- YANG, M.-C. and CUSSLER, E.L. (1986), "Designing hollow-fiber contactors", *AIChE J.* **32**, 1910-1916.